SPE · AAPG · SEG
CCUS
Carbon Capture, Utilization, and Storage

CCUS: 4436159

Optimizing CO_2 Storage in a Heterogeneous Depleted Gas Reservoir: A Case Study from the Evetts Site - Permian Basin

Millicent Okyere Williams*[1], William Ampomah[1], Najmudeen Sibaweihi[2], Adewale Amosu[2], Ryan Dupree[3], 1. Petroleum Engineering Department, New Mexico Institute of Mining and Technology, Socorro, New Mexico, USA, 2. Petroleum Recovery Research Center, Socorro, New Mexico, USA, 3. Geology & Data Analytics, Omnia Midstream Partners, Tulsa, OK, United States.

Abstract

Large-scale geological CO_2 storage in depleted gas reservoirs offers substantial potential for meeting climate mitigation targets, yet operational design in faulted systems remains insufficiently understood. Achieving commercial-scale storage requires injection strategies that effectively manage pressure buildup, plume migration, and fault-related risks. This study applies compositional flow simulation to model CO_2 injection performance in the faulted Evetts depleted gas field of the Permian Basin, with emphasis on stacked storage in the Siluro-Devonian and Fusselman–Montoya formations. A constant injection rate of 1.69 $MtCO_2$ per year over 30 years was modeled to achieve approximately 50 $MtCO_2$ of injected CO_2. Injection strategies were evaluated across variations in well injection patterns, injection formation selection, rate allocation, and fault transmissibility. Performance metrics included reservoir pressure evolution, plume migration, plume size, and the temporal evolution of hydrodynamic, residual, and solubility trapping. Results show that stacked injection combined with dual-well injection improves vertical and lateral pressure distribution, reduces maximum CO_2 gas saturation, and limits lateral plume growth relative to single-formation injection. Fault transmissibility exerts a dominant control on plume geometry and pressure propagation: open-fault scenarios enhance pressure dissipation but increase CO_2 plume contact with sealing faults while closed-fault representations confine plume migration. Among all evaluated cases, the closed-fault dual-well stacked-injection scenario stored approximately 50.7 $MtCO_2$ while maintaining a compact plume size, measuring 8.87 sq. mi at end of injection and reducing slightly to 8.40 sq. mi after 50 years of post-injection monitoring. This work provides a transferable optimization framework for designing CO_2 injection strategies in structurally complex depleted gas reservoirs and

highlights the importance of integrating fault behavior, stacked storage, and operational design parameters to minimize containment risks and long-term monitoring requirements.

Introduction

Anthropogenic CO_2 emissions continue to alter the global carbon cycle, reinforcing the need for large-scale mitigation strategies capable of achieving deep decarbonization. Carbon capture, utilization, and storage (CCUS) is a critical pathway for reducing emissions from energy production and hard-to-abate industrial sectors (Ampomah et al., 2024). To deliver meaningful climate benefits, CCUS projects must operate at commercial scale, storing tens of millions of tonnes of CO_2 safely over several decades while meeting stringent performance, containment, and monitoring requirements (IEAGHG, 2009; Jenkins, C. R. et al., 2012). Depleted gas reservoirs represent highly attractive CO_2 storage targets due to their demonstrated long-term containment, extensive subsurface characterization, and existing infrastructure (IEA GHG, 2009; Ringrose et al., 2022). However, many depleted gas fields particularly, heterogeneous carbonate systems in tectonically active basins, contain faults that introduce significant uncertainty in plume migration, pressure evolution, and long-term containment (Johannes M. Miocic et al., 2019). Fault transmissibility strongly influences the plume size and the spatial extent of pressure perturbation (Wijaya et al., 2024), making it a key operational risk factor. These uncertainties are amplified in stacked carbonate systems where vertical connectivity, formation heterogeneity, and fault architecture interact in complex ways. While previous studies have advanced understanding of CO_2 storage in saline aquifers, fewer have addressed stacked carbonate systems with realistic fault behavior, heterogeneous flow properties, and multi-well operational constraints (Ringrose et al., 2022). Recent advances highlight the need for integrated approaches that couple subsurface flow dynamics, trapping mechanisms, and deployment constraints to improve CO_2 storage performance (Ampomah et al., 2024; Boison et al., 2024, 2025a). Optimized rate allocation across stacked formations has been shown to reduce plume extent and minimize plume size in individual formations (Bodi et al., 2025), while techno-economic analyses emphasize the importance of operational efficiency in commercial-scale CCUS deployment (Koranteng et al., 2025). However, few studies have simultaneously evaluated stacked storage, multi-well injection design, and fault transmissibility within a realistic, structurally complex depleted gas reservoir. This study addresses this gap by developing a systematic evaluation framework for CO_2 storage in the faulted Evetts depleted gas field of the Permian Basin. Using high-resolution compositional simulation, we assess how injection formation selection, well injection patterns, rate allocation, and fault transmissibility jointly influence plume migration, pressure evolution, and plume size. The goal is to identify injection strategies achieving commercial-scale storage (50 $MtCO_2$) while preventing CO_2 plume contact with sealing faults, limiting plume size expansion, and ensuring long-term containment in a structurally complex carbonate reservoir.

Methodology

This study focuses on the Evetts Field in the Delaware sub-basin of the Permian Basin and employs a high-resolution three-dimensional geological model for compositional reservoir simulation. The model represents a faulted depleted gas reservoir with stacked carbonate storage formations and includes the Woodford Shale as the primary caprock, underlain by the Siluro-Devonian, Fusselman–Montoya, and Simpson formations as shown in Table 1. The Siluro-Devonian and Fusselman–Montoya formations serve as the primary CO_2 storage targets. The model spans the full structural extent of the field to a depth of ~20,000 ft. and is discretized into 206 × 219 × 47 cells (~2.57 million grid blocks), with vertical layering designed to preserve stratigraphic continuity and fault geometry. Faults intersecting the reservoir section are explicitly represented to evaluate their influence on pressure dissipation and plume migration. Initial reservoir conditions reflect a depleted gas system and were assigned using depth-dependent pressure gradients consistent with regional Permian Basin trends.

Relative permeability (Table 2) and hysteresis effects were modeled using Corey-type functions [Equations 1–2] and Land's trapping formulation [Equations 5–9]. Injection pressures were constrained using a fracture-pressure gradient of 0.62 psi/ft., with bottom-hole pressure limited to 90% of the estimated fracture pressure to maintain reservoir, caprock, and fault integrity. A base-case injection scenario was defined using a constant total injection rate of 1.69 $MtCO_2$ per year over 30 years, corresponding to a cumulative storage target of approximately 50 $MtCO_2$. CO_2 was injected as a supercritical gas, followed by a 50-year post-injection monitoring period to evaluate pressure dissipation, plume stabilization, and long-term trapping behavior.

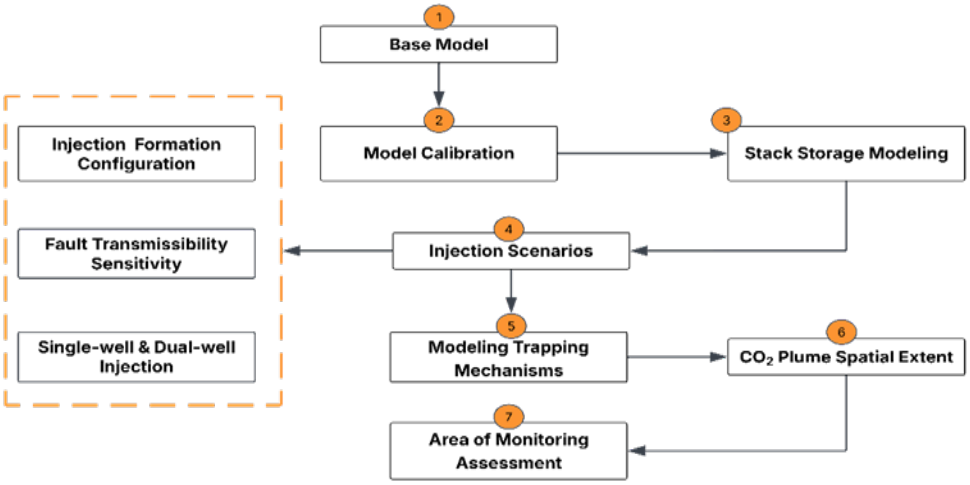

Figure 1. Workflow for Methodology

Injection scenarios were developed by varying injection using a single well and two wells, injection formation selection (single-formation vs. stacked injection), rate allocation strategy (grouped vs. split rates across wells and formations), and fault transmissibility. All scenarios maintained the same total field injection rate to ensure consistent comparison of operational performance. The plume size was defined using a gas-saturation change threshold of $\Delta Sg \geq 0.01$ [Equation 3] relative to initial conditions. Plume size was calculated [Equation 4] at end of injection (30 years) and during post-injection monitoring (10 and 50 years) to capture both peak and stabilized system behavior. These performance metrics were used to identify injection strategies that achieve the storage target while preventing CO_2 plume contact with sealing faults, limiting plume expansion, and ensuring long-term containment.

Results

The spatial evolution of the CO_2 plume was evaluated using gas-saturation (Sg) maps to delineate plume size during and after injection. Figure 2 illustrates the plan-view plume distribution at the end of the 30-year injection period for the closed-fault dual-well stacked-injection scenario. The plume remains compact around the injection wells with minimal lateral migration toward major faults, confirming effective structural containment. Across all scenarios, injection configuration strongly influenced plume geometry. Single-formation injection produced higher localized gas saturation and greater lateral plume expansion within the active formation. In contrast, stacked injection distributed CO_2 vertically across multiple formations, reducing maximum CO_2 gas saturation in any single formation and limiting plume expansion. Dual-well injection further improved performance by distributing injection rates spatially, resulting in smaller plume footprints relative to single-well cases. Fault behavior exerted a first-order control on plume evolution. Open-fault scenarios increased CO_2 plume contact with sealing faults and expanded plume extent. Closed-fault scenarios restricted lateral migration along fault planes, producing more stable plume geometries and smaller long-term monitoring footprints. Representative average pressure evolution for the cases at end of injection and 50 years post-monitoring are shown in Figure 3,

highlighting the contrast between open- and closed-fault behaviors. Figure 5 shows cumulative injected CO_2 mass confirming achievement of the 50 Mt storage target. Figure 6 shows tracer concentrations across dual-formation injection scenarios. The optimal closed-fault dual-well stacked-injection scenario achieved approximately 50.7 $MtCO_2$ stored at the end of injection and exhibited stable long-term containment. The plume measured 8.87 sq. mi at the end of injection, showed no expansion after 10 years of post-injection monitoring, and contracted slightly to 8.40 sq. mi by 50 years. This behavior is consistent with the temporal evolution of trapping mechanisms shown in Figure 4, where hydrodynamic trapping declines and residual and solubility trapping increase during post-injection stabilization. Together, these results confirm that the optimized configuration minimizes plume extent and maintains long-term containment in a structurally complex depleted gas reservoir.

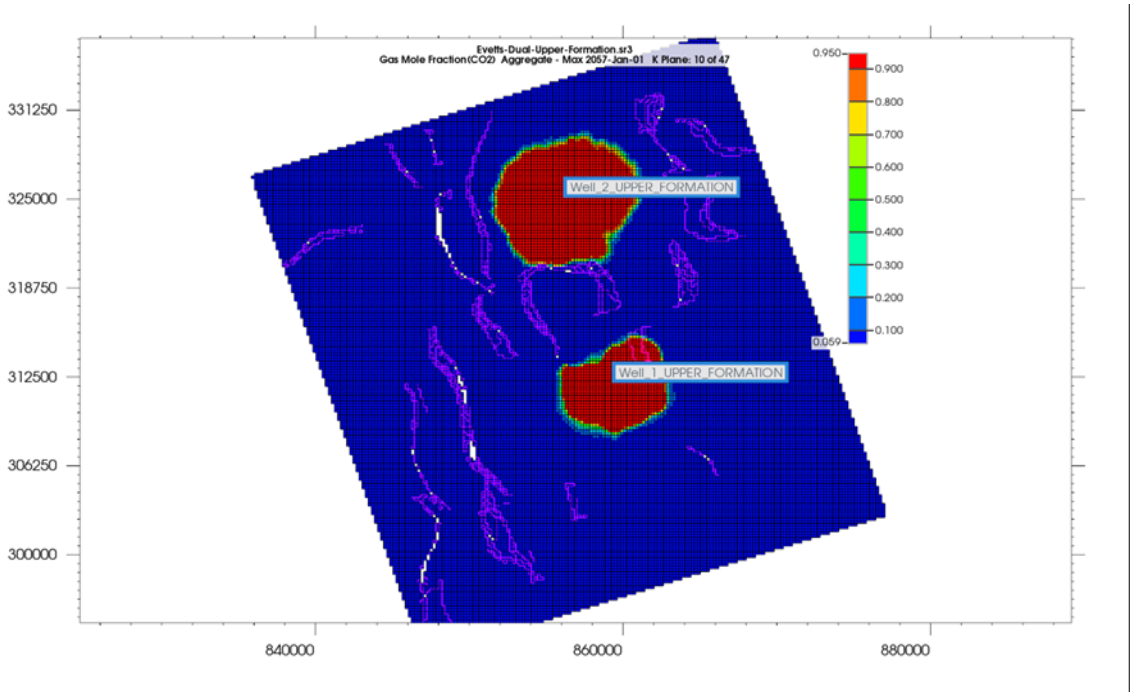

Figure 2. Plan-view gas-phase CO_2 distribution at end of injection (30 years) for the closed-fault dual-well stacked-injection case.

Conclusions

This study demonstrates that CO_2 storage performance in faulted depleted gas reservoirs is primarily controlled by injection formation selection, well placement patterns, and fault transmissibility multipliers. The dual-well stacked injection design with closed-fault representation achieved optimal storage efficiency and containment security, injecting ~50.7 $MtCO_2$ while maintaining a compact, stable plume footprint over 50 years of monitoring. Compared to single-formation and open-fault scenarios, this configuration minimized lateral plume migration, eliminated plume-fault intersection, and optimized pressure distribution across the formation stack. These findings establish a robust, transferable workflow for commercial-scale CO_2 sequestration in structurally complex depleted reservoirs. The integrated methodology (high-resolution compositional simulation coupled with multi-well injection optimization and fault transmissibility analysis) enables operators to achieve regulatory compliance, minimize monitoring obligations, maximize volumetric efficiency, and ensure long-term containment integrity in heterogeneous carbonate systems. This approach provides actionable guidance for CCUS deployment in analogous faulted, stacked-pay gas fields globally.

References

Ampomah, W., Morgan, A., Koranteng, D. O., & Nyamekye, W. I. (2024). CCUS Perspectives: Assessing Historical Contexts, Current Realities, and Future Prospects. *Energies*, *17*(17), 4248. https://doi.org/10.3390/en17174248

Miocic, J. M., Johnson, G., and Bond, C. E.: Uncertainty in fault seal parameters: implications for CO2 column height retention and storage capacity in geological CO2 storage projects, Solid Earth, 10, 951–967, https://doi.org/10.5194/se-10-951-2019

Jenkins, C. R., Cook, P. J., Ennis-King, J., Undershultz, J., Boreham, C., Dance, T., de Caritat, P., Etheridge, D. M., Freifeld, B. M., Hortle, A., Kirste, D., Paterson, L., Pevzner, R., Schacht, U., Sharma, S., Stalker, L., & Urosevic, M. (2012). Safe storage and effective monitoring of CO_2 in depleted gas fields. Proceedings of the National Academy of Sciences of the United States of America, 109(2), E35–E41. https://doi.org/10.1073/pnas.1107255108

Mishra, S., Ganesh, P. R., Schuetter, J., He, J., Jin, Z., & Durlofsky, L. J. (2015). Developing and validating simplified predictive models for CO_2 geologic sequestration. SPE Annual Technical Conference and Exhibition. https://doi.org/10.2118/175097-MS

Bodi, V.A., Ampomah, W., Bui, D., Sibaweihi, N., "Assessment of CO2 Sequestration in a Stack Storage Complex in the San Juan Basin, NM." Paper presented at the SPE Oklahoma City Oil and Gas Symposium, Oklahoma City, Oklahoma, USA, April 2025. https://doi.org/10.2118/224355-MS

Boison, P. K. N., Ampomah, W., Simmons, J. D., Bui, D., "Integrated Geochemical Modeling for CO_2 Sequestration in the San Juan Basin, New Mexico." Paper presented at the SPE Eastern Regional Meeting, Wheeling, West Virginia, USA, October 2024. https://doi.org/10.2118/221374-MS

Boison, P. K. N., Ampomah, W., Simmons, J. D., Bui, D., Sibaweihi, N., Amosu, A., & Opoku Duartey, K. (2025). Geochemical Assessment of Long-Term CO2 Storage from Core- to Field-Scale Models. Energies, 18(15), 4089. https://doi.org/10.3390/en18154089

IEA Greenhouse Gas R&D Programme. (2009). CO_2 storage in depleted gas fields (Report No. 2009/01). https://publications.ieaghg.org/technicalreports/2009-01%20Storage%20in%20Depleted%20Gas%20Fields.pdf

Koranteng, D. O., Ampomah, W., Morgan, A., and A. Ameyaw. "Design and Application of a Techno-Economic Model for CO_2 Sequestration: A Case Study of the San Juan Basin." Paper presented at the SPE Oklahoma City Oil and Gas Symposium, Oklahoma City, Oklahoma, USA, April 2025. doi: https://doi.org/10.2118/224379-MS

Ringrose, P., Guo, T., Nybråten, E., Thompson, N., Wu, L., Worthington, R., Nazarian, B., & Santi, A. (2022). Gigatonne-scale CO_2 storage: Analytical frameworks for optimizing multiple projects in sedimentary basins. First Break, 40(1), 1–5. https://doi.org/10.3997/2214-4609.202243017

Wijaya, N., Morgan, D., Vikara, D. et al. Basin-scale study of CO2 storage in stacked sequence of geological formations. Sci Rep 14, 18661 (2024). https://doi.org/10.1038/s41598-024-66272-x

Appendix A. Geological Formations

Table 1. Key geological formations in the Evetts Field model

Formation	Porosity (fraction)	Permeability (mD)	Description
Woodford Shale	0.001	0.00001	Primary Seal
Siluro-Devonian	0.130	280	Primary Storage
Fusselman	0.130	320	Primary Storage
Montoya	0.130	330	Primary Storage
Simpson	0.014	0.00001	Seal/Storage

Appendix B. Relative Permeability

Table 2 Relative Permeability Data

Parameter	Initial	Matched
Swcon, Connate water saturation (immobile water)	0.28	0.25
Swcrit, Critical water saturation (start of mobile water)	0.32	0.28
Sorw, Residual oil saturation to water (when only water is flowing)	0.3	0.3
Soirg, Irreducible oil saturation to gas	0.25	0.25
Sorg, Residual oil saturation to gas (when only gas is flowing)	0.4	0.4
Sgcrit, Critical gas saturation (minimum for mobile gas)	0.25	0.16
Sgcon, Connate gas saturation (immobile gas, if applicable)	0.10	0.15
Krogcg, Oil relative permeability at connate gas and connate water	0.45	0.45
Krwiro, Water rel. permeability at irreducible oil (maximum Krw)	1.0	0.6
Krgcl, Gas rel. permeability at connate water and residual oil(max krg)	0.66	0.98
Exp-w, Water relative permeability exponent, Nw	1.0	2.5
Exp-g, Gas relative permeability exponent, Ng	1.28	2

The following equations were used to generate data for the relative permeability curve. Corey-type gas relative permeability function (Corey, 1954) was defined in equation 1 as:

$$\text{Gas relative permeability, } Krg = Krgcl \times \left(\frac{Sg - Sgcrit}{1 - Sgcrit - Soirg - Swcon}\right)^{Ng} \quad \text{..... (1)}$$

Sg = Gas Saturation
Sgcrit = Critical gas saturation
Swcon = Connate water saturation
Soirg = Irreducible oil saturation to gas
Krgcl = Gas relative permeability at connate water and residual oil (max krg)

Corey-type water relative permeability function (Corey, 1954) was defined in Equation 1 as:

Water relative permeability, $\text{Krw} = \text{Krwiro} \times (\frac{\text{Sw}-\text{Swcrit}}{1-\text{Swcrit}-\text{Soirw}})^{\text{Nw}}$ …….…….…….……. (2)

Sw = Water saturation
Swcrit = Critical water saturation
Soirw = Irreducible oil saturation to water
Krwiro = Water rel. permeability at irreducible oil (maximum Krw)

Appendix C. Plume size Definition and Calculation

The Plume size was computed as the plan-view plume-based criteria. The plume footprint was identified using a change in gas saturation relative to initial conditions defined in Equation 3. (Bhattacharya, S., et al., 2015)

$$\Delta S_g = S_g(t) - S_{g,o} \geq 0.01 \quad \text{…….. (3)}$$

Cells satisfying $\Delta S_g \geq S_{g,cutoff}$ were classified as containing mobile CO_2.

The Plume size was calculated in equation 4 (Bhattacharya, S., et al., 2015) as:

$$Plume\ size = A_{cell} \times N_{plume-size\ cells} \quad \text{…….. (4)}$$

Where,
A_{cell} = is the areal size of a grid cell
$N_{plume-size\ cells}$ = total number of cells meeting the saturation cutoff
Plume size was evaluated at the end of injection (30 years) and during post-injection monitoring at 10 and 50 years.

Appendix D. Trapping Mechanisms

The relationship governing residual gas trapping is given by equation 5: Residual gas saturation relationship (Land, C. S. (1968)) was given by:

$$S_{grh} = S_{gcrit} + \frac{(S_{gh}-S_{gcrit})}{(1+C(S_{gh}-S_{gcrit}))} \quad \text{…….. (5)}$$

Where S_{gcrit} is the critical residual gas saturation, S_{gh} is the maximum gas saturation reached during drainage, and Land's parameter (C) is defined in Equation 6. Land's trapping coefficient (Land, C. S. (1968)) was defined as:

$$C = \frac{1}{S_{grmax}-S_{gcrit}} - \frac{1}{S_{gmax}-S_{gcrit}} \quad \text{…….…….. (6)}$$

This equation describes how historical drainage behavior affects residual gas trapping, with a higher hysteresis effect leading to more trapped CO_2. The relative permeability for gas on the drainage-to-imbibition scanning curve is given in Equation 7. Gas relative permeability with hysteresis was defined as (Land, C. S. (1968)) as:

$$K_{rg}\left(S_g\right) = K_{rg}^{dr}\left(S_{gf}\right) \quad \text{…….. (7)}$$

Where the free gas saturation S_{gf} accounts for trapped gas effects in equation 8 (Land, C. S. (1968)) as:

$$S_{gf} = S_{gcrit} + \frac{(S_g-S_{grh})(S_g-S_{gcrit})}{(S_g-S_{grh})} \quad \text{..... (8)}$$

With solubility trapping, the amount of CO_2 dissolved in formation water follows Henry's Law, which describes the proportionality between fugacity and the mole fraction of CO_2 in water defined in Equation 9 (Spycher et al., 2003). Henry's Law for CO_2 solubility was given by:

$$f_{CO_2} = y_{CO_2} H_{CO_2} \quad \text{..... (9)}$$

Where y_{CO_2} the mole fraction of CO_2 is dissolved in water, and H_{CO_2} is Henry's constant, which depends on pressure and temperature. The dependence of Henry's constant on pressure is given in Equation 10 (Spycher et al., 2003). Pressure-dependent Henry's constant is given as:

$$lnH_{CO_2} = lnH^0_{CO_2} + \frac{v^{\varphi}(P-P^*)}{RT} \quad \text{..... (10)}$$

Where $lnH^0_{CO_2}$Henry's constant at a reference pressure is the partial molar volume of CO_2 in solution, R is the gas constant, and T is the temperature.

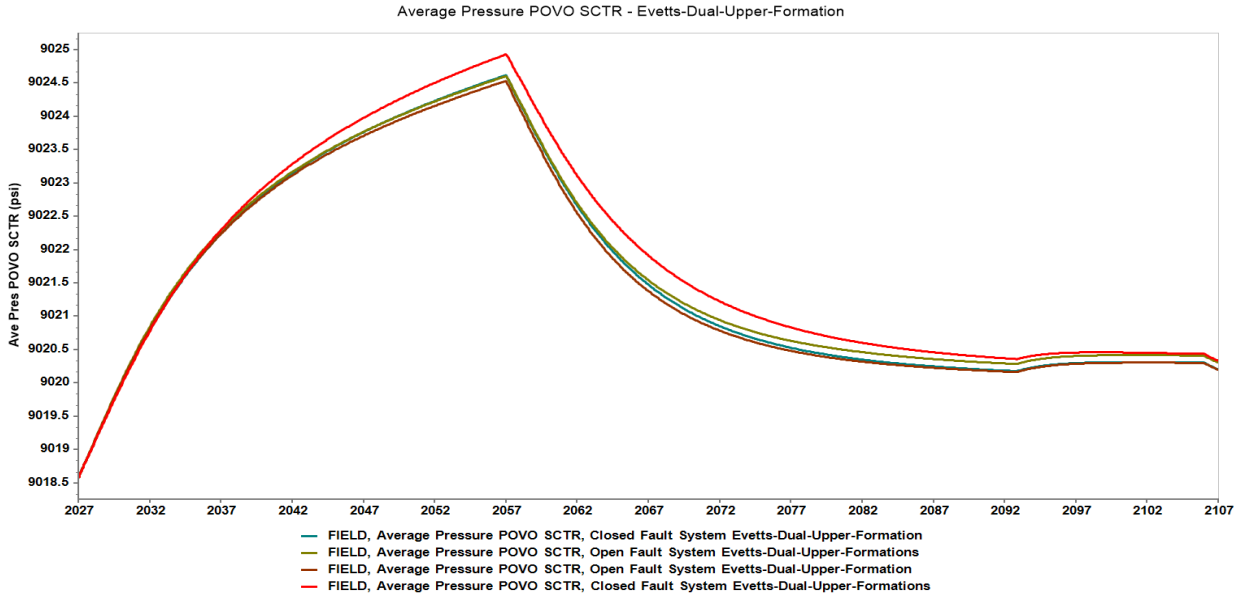

Figure 3. Plan-view pressure perturbation (psi) at end of injection (30 years) for the closed-fault dual-well stacked-injection scenario. Negative values indicate pressure increase, and positive values indicate pressure decline.

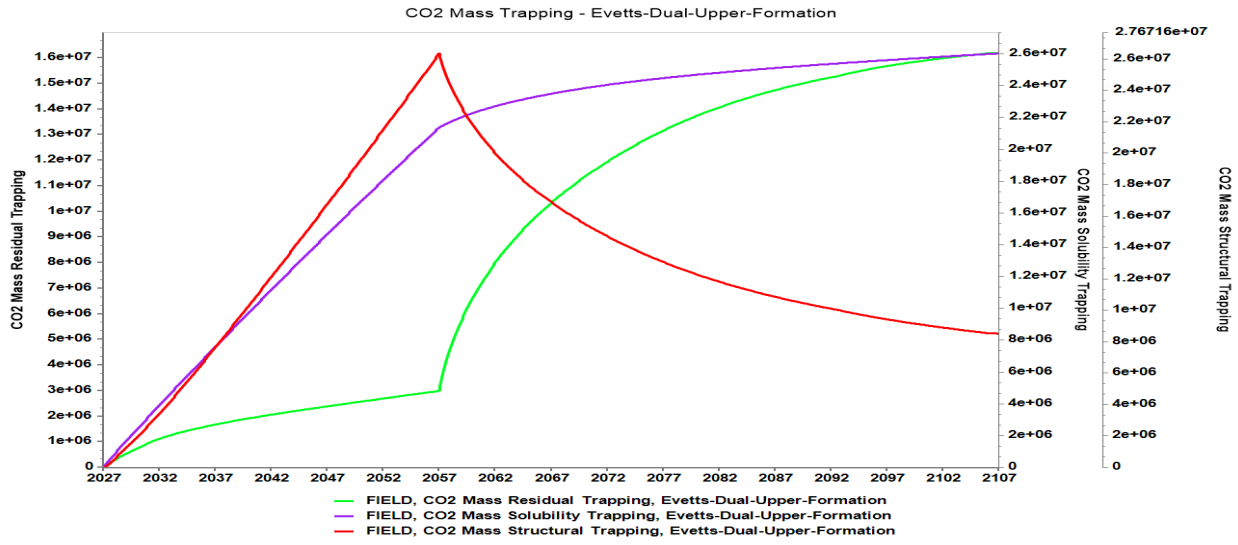

Figure 4. Temporal evolution of CO_2 mass partitioning among the trapping mechanisms for the closed-fault dual-well stacked-injection scenario.

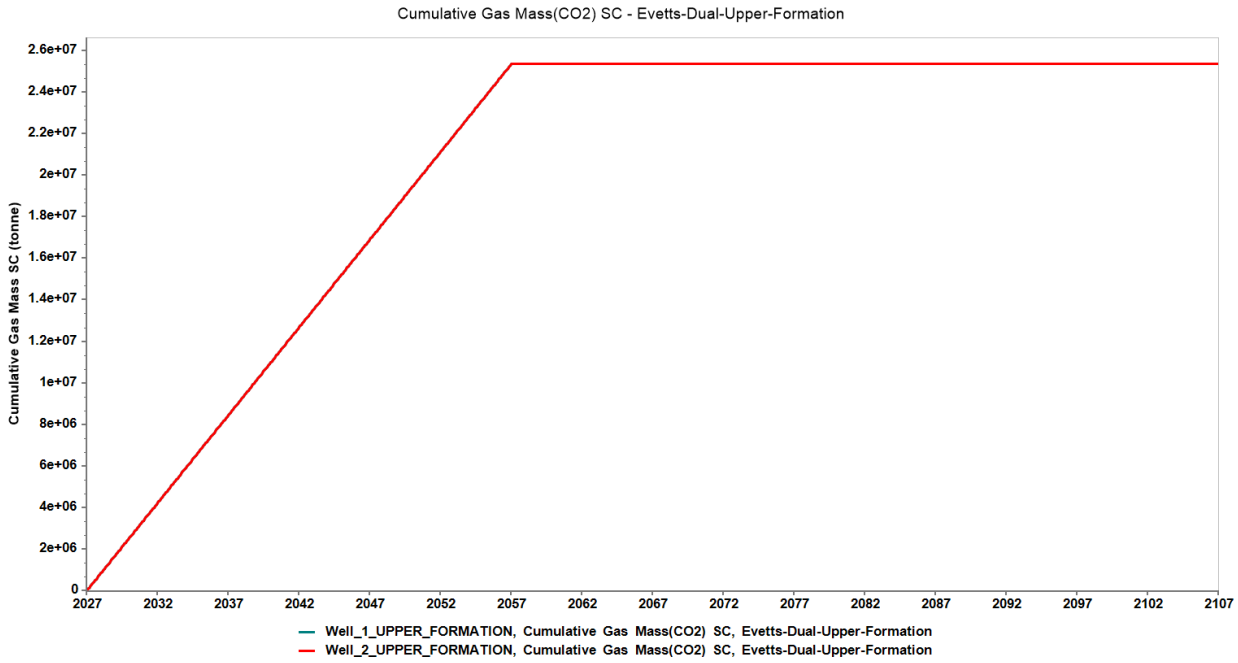

Figure 5. Cumulative injected CO_2 mass confirming achievement of the 50 Mt storage target and stable post-injection mass balance.

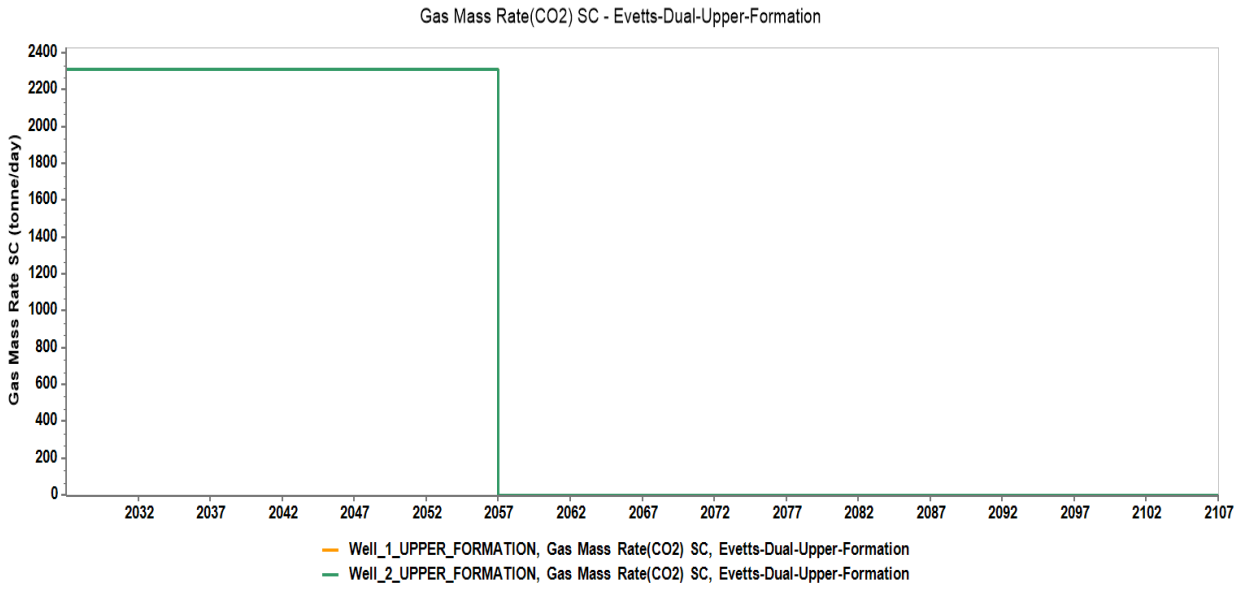

Figure 6. CO_2 Injection rate for dual-formation injection scenario.